19.

MIXING DYNAMICS OF GOLD AND SILVER ATOMIC PLUMES DURING THE SPARK ABLATION SYNTHESIS OF ALLOY NANOPARTICLES

Attila Kohut[1], Lajos Péter Villy[1], Linnéa Jönsson[2], Dániel Megyeri[1], Gábor Galbács[3], Maria E. Messing[2], Zsolt Geretovszky[1]

[1]*University of Szeged, Physics Institute, Department of Optics and Quantum Electronics, Szeged*
[2]*Lund University, Solid State Physics and NanoLund, Lund, Sweden*
[3]*University of Szeged, Department of Molecular and Analytical Chemistry, Szeged*

Introduction

Binary nanoparticles (BNPs) consist of two different materials whose combined properties – such as enhanced catalytic activity, magnetism, and optics – surpass those of single-component particles [1]. Among various synthesis methods (e.g., chemical routes, lithography, flame or laser ablation), spark ablation – or "spark mixing" – stands out for scalability: by igniting high-frequency sparks between two electrodes in a flowing gas, material from both electrodes is vaporized, mixed, and rapidly cooled into multicomponent nanoparticles [2]. Mixing can occur either inside a single spark discharge generator (so-called atomic-scale mixing) or by merging aerosols from separate generators [3]; the former is favored for its ability to tune composition and crystal structure. However, BNPs often show broad composition spreads (relative standard deviations exceeding 50%), attributed to incomplete vapor mixing and the formation of single-element primaries that later coalesce [4]. Studies using pre-alloyed electrodes or geometric constraints on vapor plumes have reduced this variability to below 10% or even 1%, underscoring the key role of vapor-phase mixing [5, 6]. Yet, direct observation of mixing dynamics has been lacking. In this work, we employ temporally- and spatially resolved optical emission spectroscopy (OES) to track gold and silver vapor expansion in the spark gap and use a quantitative model to map the Au/Ag atomic ratio over space and time during the generation of AuAg alloy nanoparticles. These measurements are compared with single-particle STEM-EDX (scanning transmission electron microscopy energy dispersive X-ray spectroscopy) analysis of the resulting AuAg BNPs to elucidate how vapor mixing governs composition uniformity.

Materials and Methods

We generated nanoparticles in a spark discharge generator (SDG) using 3 mm-diameter Au and Ag electrodes (99.99% purity) or Au–Ag alloy electrodes (50 at.% Ag, 99.99% purity). Argon carrier gas (99.996% purity) was applied flowing at 5 L/min under atmospheric pressure. Our experimental setup has been described in detail elsewhere [7]. Plasma emission was collected from a defined region in the spark gap by imaging through a lens of 80 mm diameter, and 100 mm focal length onto a 200 µm × 3 mm slit. Light passing the slit entered a 50 µm-core multimode fiber (NA 0.22) with a collimating lens, yielding ~170 µm spatial resolution along the electrode axis and 500 ns temporal resolution. The output was analyzed by an Andor Mechelle 5000 Echelle spectrograph and an iStar-734 ICCD over 300-800 nm (resolving power ~5000). Nanoparticles were collected onto TEM grids via low-pressure inertial impaction. Single-particle composition was measured by STEM-EDX on a JEOL 3000F (Inca software), with 30 particles per sample analyzed at 1-2 million× magnification. Spectra (60 s acquisition) were density- and thickness-corrected using Au and Ag L-peaks, and particle sizes were determined from pre-acquisition STEM images.

Results and Discussion

Understanding Composition and Variability in Spark-Generated BNPs

The composition of BNPs made via spark ablation can be characterized by two key metrics: the average atomic composition (e.g., Ag atomic fraction) and its variability among individual particles, expressed as the standard deviation (SD) or relative standard deviation (RSD). While ensemble techniques like ICP-MS provide average values, single-particle STEM-EDX allows assessment of

both mean and spread. For dissimilar electrodes (pure Au and Ag), the average composition is governed primarily by the relative erosion rates of the electrodes, while the variability depends on the mixing of material vapors during particle formation. A simple model, adapted from Feng *et al.*, relates composition variability (SD_φ) to the number of "smallest mixing units" (N) in a BNP [4]:

$$SD_\varphi = \sqrt{\frac{\bar{\varphi}(1-\bar{\varphi})}{N}} \qquad (1)$$

where $\bar{\varphi}$ is the average atomic composition and N is proportional to the cube of BNP size/unit size ratio. It is already evident that smaller, less mixed units yield higher variability. Two idealized scenarios were modeled to illustrate this mechanism: perfect atomic mixing (unit size ~0.15 nm) and no mixing (unit size ~4 nm). Theoretical results shown in Fig. 1A indicate that RSD decreases with increasing particle size, with perfect mixing yielding RSDs below 5% even at ~1 nm diameters, while unmixed scenarios can exceed 30% for small particles.

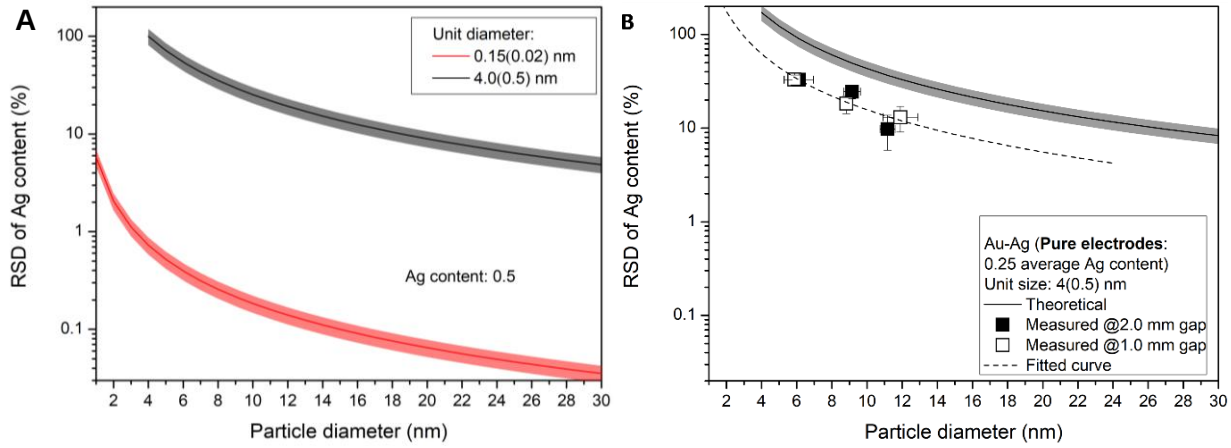

Figure 1. (A) RSD variation with the final particle diameter for two assumed unit sizes. The shaded regions around each curve indicate the uncertainty stemming from the estimated variability in unit particle diameter. (B) Measured RSD values for AuAg particles synthesized using pure Au and Ag electrodes at spark gap settings of 1.0 mm and 2.0 mm. The continuous black line represents the theoretical prediction for a mean Ag composition of 0.25 and a unit size of 4 nm (±0.5 nm). The dashed line shows the best fit of Eq. 1 to the experimental data.

Composition Spread with Pure Electrodes

Using separate Au and Ag electrodes, the BNPs exhibit relatively broad composition distributions. At a 2.0 mm interelectrode gap, the average Ag content was 0.254 with a high SD_φ of 0.079 (RSD ~31%). A size-dependent analysis of 57 particles across two spark gap settings (1.0 mm and 2.0 mm) showed that RSD decreased with increasing particle size, ranging from ~33% for 6 nm particles to ~10% for ~12 nm ones. As shown in Fig. 1B, the trend matched theoretical expectations assuming partial mixing, with a best-fit model yielding an effective unit size of ~2 nm – indicating incomplete but non-negligible vapor mixing before particle nucleation.

Mixing Dynamics Tracked by Optical Emission Spectroscopy (OES)

Time- and space-resolved OES was employed to monitor Au and Ag vapor evolution in the so-called afterglow stage of the spark. Emission measurements shown in Fig. 2A qualitatively revealed significant spatial separation of Au and Ag species in the early afterglow stage (~4.2 μs), with Ag confined near its own electrode and Au spreading more rapidly. Velocity estimates showed that the Au vapor moved ~36% faster than the Ag vapor. Full mixing (along the spark axis) occurred after ~20–25 μs, prior to significant cooling and nucleation – suggesting that mixing does occur in time to influence particle formation, though not instantaneously.

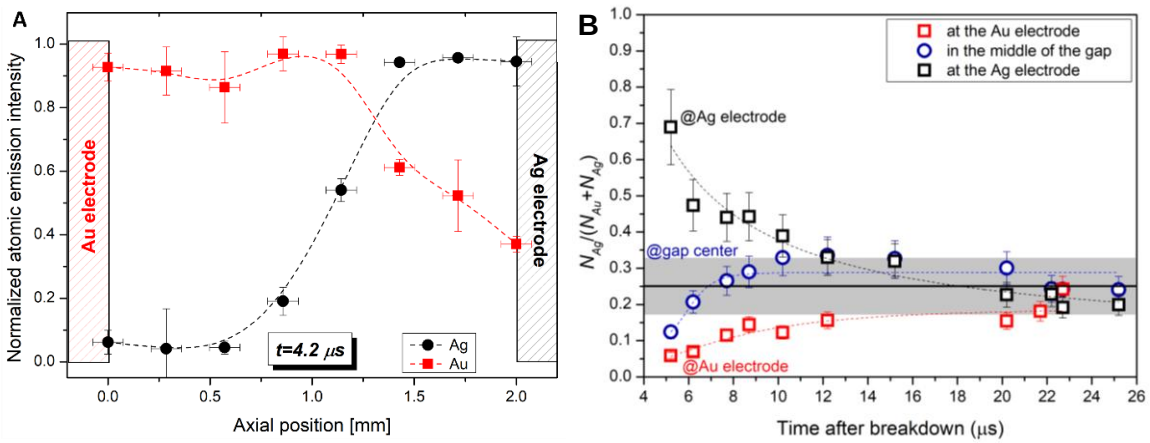

Figure 2. (A) Spatial profiles of the atomic emission intensities of Au and Ag along the spark gap, recorded 4.2 μs after the breakdown initiation. Measured points are connected to guide the eye. (B) Temporal evolution of the plasma composition – expressed as the atomic fraction of Ag – at various positions along the spark gap. The black line marks the average Ag content of the AuAg BNPs formed under identical conditions, while the shaded grey area indicates the standard deviation SD_φ of the measured BNP composition distribution.

Quantitative OES analysis – based on a self-developed model specifically tailored to this task [8] – provided the local Ag atomic fraction across the spark gap over time (Fig. 2B). Initially, strong asymmetry in vapor composition was observed (e.g., ~5% Ag near the Au electrode, ~70% near Ag), which equilibrated toward ~25% Ag across the gap by ~25 μs – closely matching the final BNP compositions measured via STEM-EDX. This supports the notion that vapor stoichiometry established during ablation is preserved through to the final particles.

Role of Lateral Vapor Expansion and Mixing Limits

Despite that OES measurements show good axial mixing, single particle STEM-EDX data indicate relatively broad composition distribution. This might be explained by that some vapor likely escapes the gap laterally before full mixing. Based on vapor jet and plasma expansion velocities (~hundreds of m/s), it is estimated that up to 20-25% of the vapor could leave the gap before equilibrium is reached. These early-escaping, unmixed or partially mixed fractions likely seed compositionally distinct primaries, contributing to broader RSD values. This explains why measured composition variability fits a partial mixing model and why the effective unit size is closer to 2 nm rather than 0.15 nm, that would correspond to perfect atomic mixing.

Implications of Electrode Gap and Vapor Confinement

Experiments at 1.0 mm gap showed slightly lower SD_φ (~0.067 vs. 0.079 at 2.0 mm), which could be due to some material transfer between electrodes (e.g., gold transferring to silver). This may enhance vapor overlap and reduce RSD, further suggesting that geometry influences mixing. Comparisons to literature (e.g., [6]) show that restricting lateral expansion – such as via funnel-like geometries – can dramatically improve mixing and reduce RSDs to ~2% for 5 nm particles, even when using pure electrodes.

Conclusions

This study investigates the spark mixing process in the Au–Ag BNP system by synthesizing and characterizing particles from both alloyed and pure Au/Ag electrodes. The composition distribution of the BNPs was analyzed using a simple statistical model, showing that particles formed from pure electrodes display size-dependent variability in composition – indicating an intermediate mixing state between fully atomic-level mixing and unmixed primary particles. Time- and space-resolved OES revealed that gold and silver vapors equilibrate along the spark axis within 20–25 μs after breakdown.

The resulting Ag/Au ratio aligns with the final BNP composition, confirming that the relative erosion rate of the electrodes governs the average particle composition. However, despite good axial mixing, substantial composition variability remains, particularly in smaller particles (e.g., ~33% RSD at 6 nm, ~10% at 11 nm). This variability is attributed to rapid plasma expansion perpendicular to the electrode axis, causing some vapor fractions to escape before fully mixing. These results suggest that to achieve highly uniform BNPs at small sizes, the mixing of vapors must occur earlier – ideally before primary particle formation. One effective strategy is to constrain vapor expansion geometrically, as supported by literature, which enhances compositional uniformity. This study provides mechanistic insight into such effects, offering guidance for optimizing SDG designs for controlled BNP synthesis. Further details on this topic can be found in our related publication [9].

References

[1] M. Rebello Sousa Dias and M. S. Leite, *Acc Chem Res*, 2019, **52**, 2881–2891.
[2] Andreas. Schmidt-Ott, Ed., *Spark Ablation: Building Blocks for Nanotechnology*, Jenny Stanford Publishing, 2020.
[3] T. V. Pfeiffer, J. Feng and A. Schmidt-Ott, *Advanced Powder Technology*, 2014, **25**, 56–70.
[4] J. Feng, N. Ramlawi, G. Biskos and A. Schmidt-Ott, *Aerosol Sci Technol*, 2018, **52**, 505–514.
[5] L. Jönsson, M. Snellman, A. C. Eriksson, M. Kåredal, R. Wallenberg, S. Blomberg, A. Kohut, L. Hartman and M. E. Messing, *J Aerosol Sci*, 2024, **177**, 106333.
[6] D. O. de Zárate, C. García-Meca, E. Pinilla-Cienfuegos, J. A. Ayúcar, A. Griol, L. Bellières, E. Hontañón, F. E. Kruis and J. Martí, *Nanomaterials 2020, Vol. 10, Page 466*, 2020, **10**, 466.
[7] L. P. Villy, A. Kohut, A. Kéri, Á. Bélteki, G. Radnóczi, Z. Fogarassy, G. Z. Radnóczi, G. Galbács and Z. Geretovszky, *Sci Rep*, 2022, **12**, 1–9.
[8] A. Kohut, L. P. Villy, G. Kohut, G. Galbács and Z. Geretovszky, *Appl Spectrosc*, 2023, **77**, 1401–1410.
[9] A. Kohut, L. P. Villy, L. Jönsson, D. Megyeri, G. Galbács, M. E. Messing, Zs. Geretovszky, *Nanoscale Adv*, 2025, **7**, 3322-3330.

Acknowledgments

We are grateful for the funding provided from the National Research, Development and Innovation Fund under the PD_21 OTKA (project PD 139077) and under the 2022-2.1.1-NL Creation of National Laboratories, Complex Development funding schemes (project 2022-2.1.1-NL-2022-00012). Research leading to these results has also received funding from the K 146733 (OTKA) project and was also supported by the Swedish Foundation for Strategic Research (Grant No. FFL18–0282).